CHEMISTRY
A EUROPEAN JOURNAL

DOI: 10.1002/chem.200600469

Carbon Nanotube/Poly(methyl methacrylate) (CNT/PMMA) Composite Electrode Fabricated by In Situ Polymerization for Microchip Capillary Electrophoresis

Xiao Yao,[a, c] Huixia Wu,[a, c] Joseph Wang,[b] Song Qu,[a] and Gang Chen*[a]

Abstract: We describe the development and application of a novel carbon nanotube/poly(methyl methacrylate) (CNT/PMMA) composite electrode as a sensitive amperometric detector of microchip capillary electrophoresis (CE). The composite electrode was fabricated by the in situ polymerization of a mixture of CNTs and prepolymerized methyl methacrylate in the microchannel of a piece of fused silica capillary under heat. The performance of this unique system was demonstrated by the separation and detection of phenolic pollutants and purines. The new CNT-based CE detector offered significantly lower operating potentials, yielded substantially enhanced signal-to-noise characteristics, and exhibited resistance to surface fouling and, hence, enhanced stability. Long-term stability and reproducibility with relative standard deviations of less than 5% for the peak current ($n=20$) were also demonstrated. The simplicity and significant performance exhibited by the CNT/PMMA composite electrode indicate great promise for conventional CE, flowing-injection analysis, and other microfluidic analysis systems.

Keywords: electrochemistry · electrophoresis · nanotubes · poly(methyl methacrylate) · purines

Introduction

Since Iijima reported the existence of carbon nanotubes (CNT) in 1991,[1] they have attracted much attention because of their high electrical conductivity, mechanical strength, and chemical stability.[2,3] The unique properties of CNTs make them extremely attractive for electrochemical sensors and biosensors.[4–6] Recent investigations demonstrated that CNTs show strong electrocatalytic activity and minimization of surface fouling if employed to improve the electrochemical response of some important bioactive substances.[7–10] A variety of carbon-nanotube electrodes have been fabricated for sensing different redox compounds, for example, CNT-modified screen-printed carbon electrode,[11] CNT-powder microelectrode,[12] CNT/Teflon composite electrode,[13] CNT screen-printed electrode,[14] CNT/epoxy composite electrode,[15] and CNT/copper composite electrode.[16] The commonly used approach for fabricating CNT electrodes is surface modification. To load CNTs onto the surface of electrodes, CNTs were usually dispersed in solvents[17,18] or polymer solutions (such as Nafion[19] and chitosan[20] solutions) that were cast on the electrodes, because CNTs were insoluble in most solvents. Recently, methods based on electrochemical deposition[21] and electrochemical polymerization[22,23] have been employed for loading CNTs onto electrodes. CNT-based electrodes have been demonstrated to reduce the overpotential significantly.[4,21] The ability of carbon nanotubes to promote electron-transfer reactions suggests great promise for amperometric sensors.[4]

During the past decade, microfluidic analytical systems have undergone considerable development. Much attention has been paid to capillary electrophoresis (CE) microchips, due to their advantages of high performance, design flexibility, reagent economy, high throughput, miniaturization, and automation.[24–27] These microchip analysis systems hold considerable promise for biomedical and pharmaceutical analysis, clinical diagnostics, environmental monitoring, and for-

[a] X. Yao, Dr. H. Wu, S. Qu, Dr. G. Chen
Department of Chemistry, Fudan University
Shanghai 200433 (China)
Fax: (+86) 21-6564-1740
E-mail: gangchen@fudan.edu.cn

[b] Prof. J. Wang
Departments of Chemical & Materials Engineering and Chemistry
Arizona State University, Tempe, AZ 85287–5001 (USA)

[c] X. Yao, Dr. H. Wu
These authors contributed equally to this work.

Supporting information for this article is available on the WWW under http://www.chemeurj.org/ or from the author; Figures illustrating the fabrication process of the composite electrode, a 3-D adjustable device for microchip CE-AD, and high-resolution SEMs of graphite/PMMA and CNT/PMMA composites.

ensic investigations.[24–28] They can dramatically change the scale and speed at which chemical analysis is performed. Electrochemical detection (ECD), mainly in the mode of amperometric detection (AD), offers great promise for CE microchips, with features that include high sensitivity, inherent miniaturization of both the detector and control instrumentation, low cost, low power demands, and high compatibility with micromachining technologies.[29–31] The performance of microchip CE-AD is strongly influenced by the working-electrode material. The working electrode should provide favorable signal-to-background characteristics, as well as a reproducible response. A range of materials, such as platinum, gold, and various forms of carbon, have, thus, been found useful for chip-based electrochemical detection.[32–35]

Poly(methyl methacrylate) (PMMA) is a versatile polymer of low price, excellent optic transparency, and excellent electric and mechanical properties.[27,36] CNT/PMMA composites have been prepared by solvent evaporation,[37] melt mixing,[38] and in situ polymerization.[39] Recent investigations have focussed mainly on its electrical properties.[37–39] To the best of our knowledge, there have been no reports on the fabrication of CNT/PMMA composite electrodes for electrochemical sensing.

In this work, a CNT/PMMA composite microdisc electrode was fabricated by in situ polymerization and employed as the end-column amperometric detector of a microchip CE system. The fabrication details, characterization, feasibility, and performance of the novel CNT/PMMA composite electrode were demonstrated by monitoring phenolic pollutants and purines in connection with microchip CE.

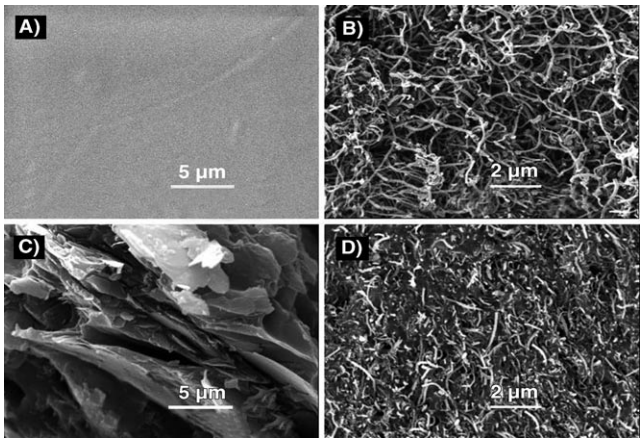

Figure 1. SEM images of the surfaces of A) pure PMMA sheet, B) pure CNTs, and the cross sections of C) graphite/PMMA and D) CNT/PMMA composites. Conditions: accelerating voltage, 20 kV; magnification, ×5000 (A,C), ×10000 (B,D).

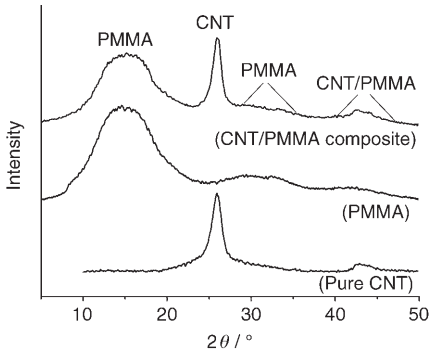

Figure 2. XRD patterns of CNTs, PMMA, and the CNT/PMMA composite.

Results and Discussion

The graphite/PMMA and the CNT/PMMA composite electrodes were directly fabricated within the bore of a fused silica capillary (320 μm i.d., 450 μm o.d.), due to the size compatibility of the electrode and the channel outlet (20 μm deep, 50 μm wide). This provided a simple way to prepare the detection electrodes for microchip CE. Figure 1 shows SEM images of the surface of a pure PMMA sheet (A), pure CNTs (B), and the cross sections of the 40 wt. % graphite/PMMA (C) and the 40 wt. % CNT/PMMA (D) composites. It is clear from Figure 1D that the carbon nanotubes are dispersed and embedded throughout the PMMA matrix and an interconnected carbon-nanotube network has formed. This conductive nanotube network may establish electrical conduction pathways throughout the whole system, which is responsible for the electric conductivity and electrochemical sensing. Figure 1C indicates that the sheet-like structure of graphite still exists in the graphite/PMMA composite. Figure S3 of the Supporting Information illustrates the high-resolution SEM images of the cross sections of graphite/PMMA and CNT/PMMA composites.

Figure 2 displays the X-ray diffraction (XRD) patterns of CNTs and the CNT/PMMA composite. Diffraction peaks assigned to CNTs at 25.9 and 42.7° (corresponding to the graphite indices of (002) and (100))[40] are seen clearly for both pure CNTs and the CNT/PMMA composite, indicating that the CNT structure was not destroyed after the in situ polymerization of methyl methacrylate (MMA). The three broad, characteristic peaks of PMMA were also observed in the XRD pattern of the CNT/PMMA composite, however, the second peak of CNT merges with the third peak of PMMA. Because the MMA monomer will evaporate during the in situ polymerization, thermogravimetry (TGA) was employed to evaluate the weight fraction of CNTs in the CNT/PMMA composite. Figure 3 shows TGA curves of CNTs and the CNT/PMMA composite under nitrogen at a heating rate of 10 °C min^{-1}. PMMA starts to degrade at around 200 °C and decomposes almost completely at 405 °C,[41] whereas only 3.0 % of CNTs decompose at this temperature. Weight loss of the composite occurred between 250 and 350 °C due to the decomposition of PMMA. From the TGA curves of the CNT/PMMA composite, the weight fraction of CNTs in the CNT/PMMA composite was estimated to be approximately 48 %.

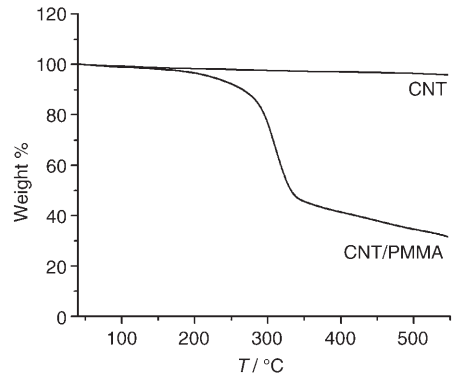

Figure 3. Thermogravimetric curves of CNTs and the CNT/PMMA composite.

Figure 4 illustrates the cyclic voltammograms (CV) of 4-chlorophenl. The half-wave potentials of the anode peak for the oxidation of 4-chlorophenol are approximately +0.5 and +0.3 V (vs. Ag/AgCl wire) at the graphite/PMMA and CNT/PMMA composite electrodes, respectively. The catalytic activity of the CNT-based electrode is evident from the substantial negative shift of the half-wave potential and the significantly enhanced current signal for the oxidation of 4-chlorophenl relative to the graphite/PMMA electrode. Apparently, the CNT/PMMA composite greatly promotes the oxidation process of 4-chlorophenol.

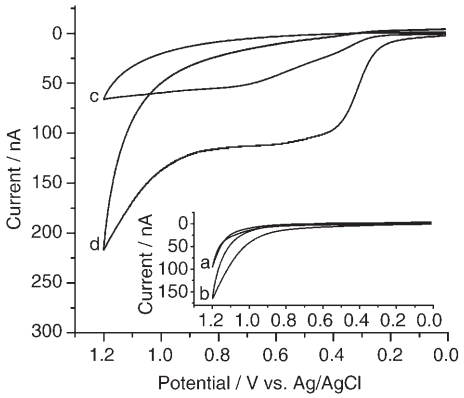

Figure 4. Cyclic voltammograms of the graphite/PMMA electrode (a,c) and the CNT/PMMA composite electrode (b,d) in 40 mM borate buffer (pH 9.8) in the absence (a,b) and presence (c,d) of 1 mM 4-chlorophenol. Scan rate, 100 mV s^{-1}.

Here, the CNT/PMMA composite microdisc electrode was coupled with a microchip CE system as an end-column amperometric detector. The attractive performance of the detector is indicated by the detection of eight phenols of environmental concern. This system offers enhanced sensitivity, low noise levels, and well-resolved peaks. Figure 5 shows representative electropherograms for 2,6-dimethylphenol (a), phenol (b), 2-naphthol (c), 4-chlorophenol (d), pentachlorophenol (e), 2,4-chlorophenol (f), 3-nitrophenol (g), and 4-nitrophenol (h) recorded with graphite/PMMA (A) and CNT/PMMA (B) composite electrode detectors. The eight phenols can be separated with the CNT/PMMA composite electrode to give well-defined and resolved peaks within 200 s. Broader peaks (and, hence, inferior resolution) are observed at the graphite/PMMA detector. The sharp and well-resolved responses at the CNT/PMMA detector result in smaller values of the half-peak widths for 2,6-dimethylphenol, phenol, 2-naphthol, 4-chlorophenol, pentachlorophenol, 2,4-chlorophenol, 3-nitrophenol, and 4-nitrophenol at the CNT/PMMA electrode relative to the graphite/PMMA electrode (3.9 vs. 5.1, 3.9 vs. 4.5, 3.9 vs. 4.6, 3.8 vs. 4.8, 4.4 vs. 5.5, 4.2 vs. 5.1, 4.9 vs. 7.3, and 5.8 vs. 9.1 s, respectively). The exact reason for the sharper peaks observed at the CNT-modified electrode is not fully understood at this stage.[42] Additionally, the surface fouling of the graphite-based electrode may contribute to wider peaks than those for the CNT-based electrodes, which are known to minimize such fouling effects.[11] Furthermore, the current signals of these phenolic compounds at the CNT/PMMA composite electrode are higher than those at the graphite/PMMA detector.

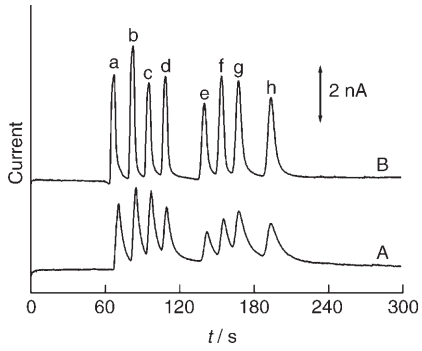

Figure 5. Electropherograms for mixtures containing a) 50 μM 2,6-dimethylphenol, b) 50 μM phenol, c) 50 μM 2-naphthol, d) 50 μM 4-chlorophenol, e) 100 μM pentachlorophenol, f) 100 μM 2,4-chlorophenol, g) 100 μM 3-nitrophenol, and h) 100 μM 4-nitrophenol at A) the graphite/PMMA and B) the CNT/PMMA composite microdisc electrodes. The separation channel in the glass CE microchip was 50 μm wide × 20 μm deep × 74 mm long; separation and injection voltage, +2500 V; injection time, 3 s; running buffer, 40 mM borate buffer (pH 9.8); detection potential, +0.8 V (vs. Ag/AgCl wire).

In addition, the CNT/PMMA composite electrode also exhibits high electrocatalytic activity toward the oxidation of purines. Figure 6 shows representative electropherograms for guanine and xanthine recorded with graphite/PMMA (A) and CNT/PMMA composite (B) electrode detectors. Broader peaks and inferior resolution are observed at the graphite/PMMA detector. The sharp and well-resolved responses at the CNT/PMMA detector reflect its lower surface fouling. The ability of carbon nanotubes to promote electron-transfer reactions on the electrode has been attributed to their special electronic structure and high electrical conductivity.[6,11]

The present CNT/PMMA composite electrode shows low-noise characteristics and a stable baseline, which is not always the case for other CNT electrodes in CE or micro-

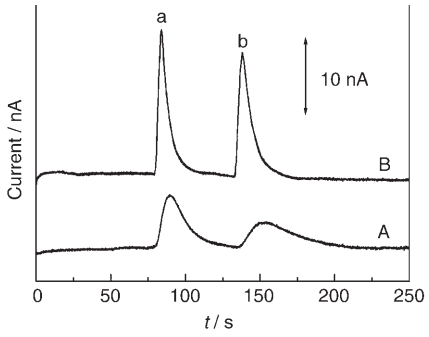

Figure 6. Electropherograms for mixtures containing a) 100 μM guanine and b) 200 μM xanthine at A) the graphite/PMMA and B) the CNT/PMMA composite microdisc electrodes. Separation and injection voltage, +1500 V; injection time, 3 s; running buffer, 10 mM borate/20 mM phosphate buffer (pH 8.0); detection potential, +0.8 V (vs. Ag/AgCl wire).

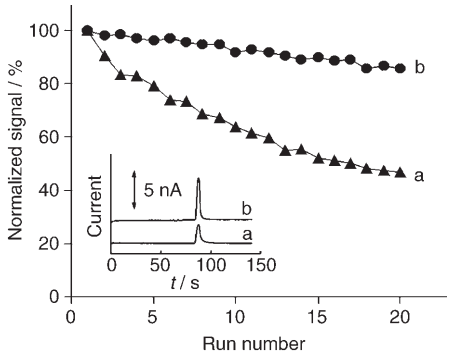

Figure 7. Stability of the response for repetitive measurements of 50 μM phenol at a) the graphite/PMMA and b) the CNT/PMMA composite microdisc electrodes. Also shown (insets) are the first electropherograms of 50 μM phenol at a) the graphite/PMMA and b) the CNT/PMMA composite microdisc electrodes. Conditions, as in Figure 5.

chip CE, such as CNT-coated electrodes[11,43] and CNT-paste electrodes.[16,44] The present CNT/PMMA electrode has a significant advantage over these other CNT electrodes because it is rigid and stable and is not prone to wearing over time. Its low noise level may be attributed to the stable and rigid conductive network of the CNT/PMMA composite. The enhanced current response of the CNT/PMMA composite electrode can be ascribed to not only the electrocatalytic activity of CNTs, but also the higher surface area of the CNT composite. In this work, the performances of CNT/PMMA and graphite/PMMA composite electrodes were compared to demonstrate the advantages of CNTs for electrochemical sensing in combination with CE microchip. Recently, Compton's group demonstrated significantly that both CNT-based electrodes and edge-plane pyrolytic graphite electrodes showed similar electrocatalytic activity toward a range of redox systems, whereas basal-plane pyrolytic graphite electrodes displayed low activity, indicating that the edge-plane sites of edge-plane pyrolytic graphite electrodes were electroactive sites.[6,45,46] In this work, the graphite/PMMA composite electrode was made from a mixture of graphite powder and prepolymerized MMA. A great deal of edge-plane sites of graphite were embedded in the composite so that the electrocatalytic activity of the graphite/PMMA composite electrode was poor, resulting in lower current response. As shown in Figure 1D, the CNTs (30–60 nM diameter) on the surface of the composite function like thousands of nanoelectrodes. The mass transfer on the CNT-electrode network is much faster than that on the microsized graphite on the surface of the graphite/PMMA composite, with the effect that the current response was enhanced to some extent.

The electrocatalytic detection on the CNT/PMMA composite electrode is coupled to resistance to surface fouling and, hence, to good stability. Such improvements were illustrated by the CE microchip measurements of phenol, known to promote surface passivation. Figure 7 displays the response of the graphite/PMMA (a) and CNT/PMMA (b) detectors to 20 repetitive CE measurements of 50 μM phenol. The initial response was found to drop off gradually at the graphite-based detector, with a decrease of 53% (RSD of 24.9%, $n=20$). In contrast, a stable response (RSD of 4.7%, $n=20$), with a very slow decrease in the response (up to 14.2%) is observed over the entire operation for the CNT-based detector. The good stability is coupled to a reproducible response. The precision of peak currents was examined from a series of eight repetitive injections of mixtures containing 25 μM 2,6-dimethylphenol (a), 25 μM phenol (b), 25 μM 2-naphthol (c), 25 μM 4-chlorophenol (d), 50 μM pentachlorophenol (e), 50 μM 2,4-chlorophenol (f), 50 μM 3-nitrophenol (g), and 50 μM 4-nitrophenol (h) that yielded highly reproducible signals with RSDs of 3.4, 3.8, 3.3, 4.4, 3.2, 3.7, 4.2, and 4.4%, respectively (conditions, as in Figure 5). The higher antipassivation capability of the CNT/PMMA composite can be attributed to its lower roughness relative to the graphite/PMMA composite, as shown in Figure 1.

Figure 8 depicts the typical hydrodynamic voltammograms for the oxidation of 25 μM phenol on the graphite/PMMA (a) and CNT/PMMA (b) composite microelectrodes. The curves were recorded pointwise over the +0.1 to +1.0 V (vs. Ag/AgCl wire) range by changing the applied potential

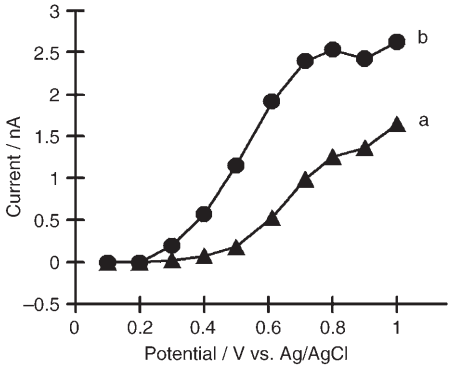

Figure 8. Hydrodynamic voltammograms for 25 μM phenol at a) the graphite/PMMA and b) the CNT/PMMA composite microdisc electrodes. Conditions, as in Figure 5.

by 0.1 V. The current response of the CNT-composite electrode is higher than that of the graphite-based electrode at the same potential, although the geometric areas of the two electrodes are the same. As the applied potential exceeds +0.50 V for the graphite/PMMA (a) and +0.30 V for CNT/PMMA (b), the peak current of both electrodes rises rapidly. However, the current response increases much more slowly as the potential exceeds +0.80 V for graphite/PMMA (a) and +0.70 V for CNT/PMMA (b). The detection potential of the CNT-based electrode was, therefore, maintained at +0.80 V, under which condition the background current was not too high and the signal-to-noise ratio was the highest. The half-wave potentials at the graphite/PMMA (a) and CNT/PMMA (b) composite microdisc electrodes are +0.64 and +0.49 V, respectively, for the oxidation of phenol. The electrocatalytic activity toward the investigated analyte is pronounced, as the half-wave potentials on the CNT-based electrode have decreased by 150 mV relative to that on the graphite/PMMA composite electrode, indicating that the CNT-based electrodes allow amperometric detection with higher sensitivity and at significantly lower operating potentials. Overall, the data given above indicate that the CNT/PMMA composite is a promising material for electrochemical sensing.

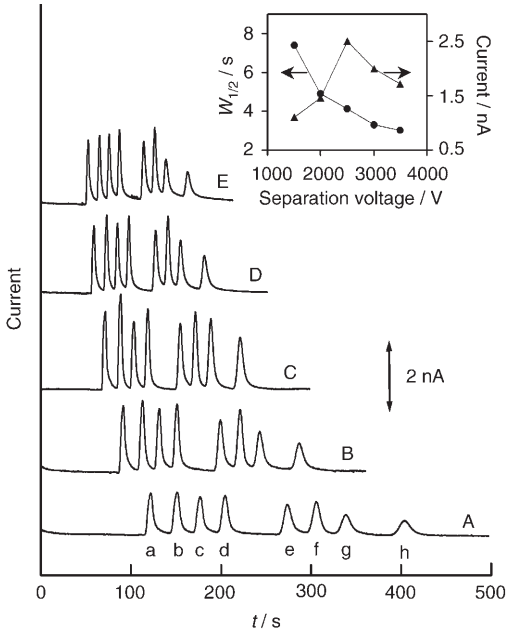

Figure 9. Electropherograms for mixtures containing a) 25 μM 2,6-dimethylphenol, b) 25 μM phenol, c) 25 μM 2-naphthol, d) 25 μM 4-chlorophenol, e) 50 μM pentachlorophenol, f) 50 μM 2,4-chlorophenol, g) 50 μM 3-nitrophenol, and h) 50 μM 4-nitrophenol at the CNT/PMMA composite electrode at the separation of voltage of A) +1500 V, B) +2000 V, C) +2500 V, D) +3000 V, and E) +3500 V. Also shown (inset) are the effects of separation voltage upon the peak current and half-peak width ($W_{1/2}$) of phenol. Conditions, as in Figure 5.

Figure 9 shows the electropherograms for mixtures containing 25 μM 2,6-dimethylphenol (a), 25 μM phenol (b), 25 μM 2-naphthol (c), 25 μM 4-chlorophenol (d), 50 μM pentachlorophenol (e), 50 μM 2,4-chlorophenol (f), 50 μM 3-nitrophenol (g), and 50 μM 4-nitrophenol (h) at the separation voltages of (A) +1500, (B) +2000, (C) +2500, (D) +3000, and (E) +3500 V. As expected, increasing the separation voltage from +1500 to +3500 V (A–E) dramatically decreases the migration time from 121.8 to 52.5, 151.1 to 65.2, 176.6 to 75.9, 204.5 to 87.2, 273.5 to 113.9, 305.3 to 126.5, 338.7 to 138.8, and 403.2 to 162.9 s, respectively. Also shown (inset) are the effects of the separation voltage upon the peak current and half-peak width ($W_{1/2}$) of phenol. Upon raising the separation voltage from +1500 to +3500 V, the peak current of phenol increases to the maximum value of 2.49 nA (at +2500 V) and decreases gradually to 1.71 nA (at +3500 V) and the half-peak width ($W_{1/2}$) of phenol significantly decreases from 7.4 to 3.0 s. Notice also the flat baseline current even at high separation voltages. Such a behavior indicates the effective isolation of the CNT/PMMA electrode from the high separation voltage. Moreover, higher separation voltages may result in higher Joule heat that directly affects the separation efficiency of this method. However, too-low separation voltages will increase the analysis time considerably, which in turn causes peak broadening. Based on experiments, +2500 V was chosen as the optimum voltage to accomplish a good compromise, considering the resolution, sensitivity, and analysis time.

The CNT/PMMA composite electrode detector offers a well-defined concentration dependence. Electropherograms for mixtures containing increasing levels of 2,6-dimethylphenol (a), phenol (b), 4-chlorophenol (c), and 2,4-chlorophenol (d) in increments of 10 μM (for a–c) and 20 μM (for d) at the CNT/PMMA composite microdisc electrodes are shown in Figure 10 (A–E). Defined peaks, proportional to the concentration of the four phenols, are observed. The resulting calibration plots (insets) are highly linear, with sensitivities of 84.2, 99.7, 73.5, and 37.6 nA mM^{-1} for 2,6-dimethylphenol (a), phenol (b), 4-chlorophenol (c), and 2,4-dichlorophenol (d), respectively (correlation coefficients, 0.9996, 0.9994, 0.9997, and 0.9991). The detection limits of 0.011 μM 2,6-dimethylphenol, 0.009 μM phenol, 0.012 μM 4-chlorophenol, and 0.024 μM 2,4-dichlorophenol were estimated based on a signal-to-noise ratio of 3, indicating the favorable signal-to-noise characteristics of the CNT/PMMA composite electrode. Such values are much better than the detection limits obtained (1–2 μM) by using a gold-coated screen-printed carbon-line electrode.[32]

The suitability of the CNT/PMMA composite electrode for measuring low levels of phenolic pollutants in relevant environmental samples is demonstrated in Figure 11. The electropherogram for a river-water sample, spiked with 5 μM 2,6-dimethylphenol (a), 5 μM phenol (b), 5 μM 2-naphthol (c), 5 μM 4-chlorophenol (d), 10 μM pentachlorophenol (e), 10 μM 2,4-chlorophenol (f), 10 μM 3-nitrophenol (g), and 10 μM 4-nitrophenol (h) is characterized by eight well-defined and baseline-resolved peaks. As shown in Figure 11A, none of the investigated eight phenolic pollutants was detected in the river water. The standard-spiked river water

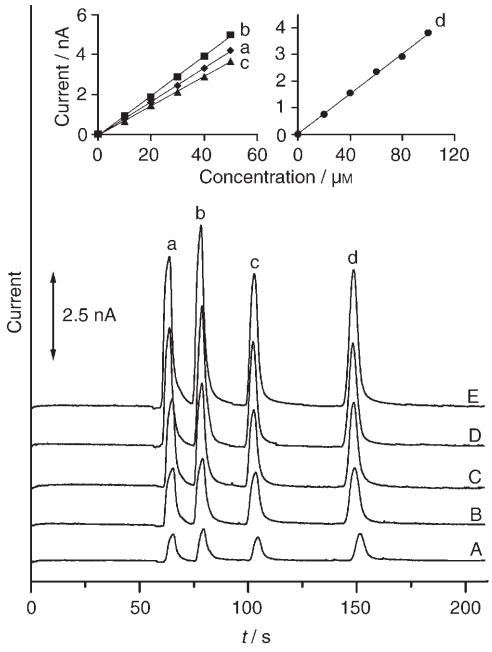

Figure 10. Electropherograms for mixtures containing increasing levels of a) 2,6-dimethylphenol, b) phenol, c) 4-chlorophenol, and d) 2,4-chlorophenol in increments of 10 μM (a–c) and 20 μM (d) at the CNT/PMMA composite electrode. Also shown (insets) are the resulting calibration plots. Other conditions, as in Figure 5.

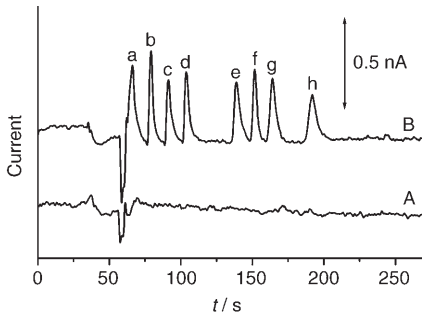

Figure 11. Electropherograms for a river-water sample A) before and B) after addition of a) 5 μM 2,6-dimethylphenol, b) 5 μM phenol, c) 5 μM 2-naphthol, d) 5 μM 4-chlorophenol, e) 10 μM pentachlorophenol, f) 10 μM 2,4-chlorophenol, g) 10 μM 3-nitrophenol, and h) 10 μM 4-nitrophenol at the CNT/PMMA composite electrode. Other conditions, as in Figure 5.

was analyzed under the optimum conditions (Figure 11B). The average recoveries and RSDs were 92.6 and 2.0% for 2,6-dimethylphenol, 98.4 and 1.2% for phenol, 95.6 and 2.2% for 2-naphthol, 101.6 and 2.1% for 4-chlorophenol, 95.9 and 1.8% for pentachlorophenol, 102.8 and 2.6% for 2,4-chlorophenol, 94.3 and 4.5% for 3-nitrophenol, and 96.1 and 4.8% for 4-nitrophenol ($n=3$). The results demonstrated that this method is both highly accurate and very precise for the analytes tested in the real sample.

Conclusion

We have developed a new approach based on in situ polymerization for the fabrication of a CNT/PMMA composite electrode as the end-column amperometric detector of microchip CE. The performance, utility, and advantages of the novel set-up were demonstrated in combination with the separation and detection of phenolic pollutants and purines. This system is characterized by its high resolution and sensitivity, low operation costs, and requirements for low amounts of sample. The new CNT-based CE detector offers favorable signal-to-background characteristics, good resistance to surface fouling, strong electrocatalytic activity, sharp peaks for the analytes, and simple design and fabrication. This new microchip protocol offers great promise for a wide range of environmental and bioanalytical applications.

Experimental Section

Reagents and solutions: Multiwall carbon nanotubes (MWCNT, 30–60 nM diameter, 5–15 μm long), with a purity of 95%, were provided by Shenzhen Nanoport Company (Shenzhen, China). Methyl methacrylate (MMA), 2-2′-azo-bisisobutyronitrile (AIBN), borax, 2,6-dimethylphenol, phenol, 2-naphthol, 4-chlorophenol, pentachlorophenol, 2,4-chlorophenol, 3-nitrophenol, 4-nitrophenol, guanine, and xanthine were all purchased from SinoPharm (Shanghai, China). The graphite powder was supplied by Aldrich (Wilwaukee, WI, USA). Other chemicals were all of analytical grade.

Stock solutions of 2,6-dimethylphenol, phenol, 2-naphthol, 4-chlorophenol, pentachlorophenol, 2,4-chlorophenol, 3-nitrophenol, and 4-nitrophenol (20 mM) were prepared in 50% aqueous ethanol. The stock solutions of guanine and xanthine (10 mM) were made in water.

Electrode fabrication: The fabrication process for the composite electrodes is illustrated in the Supporting Information, Figure S1. Prior to fabrication, 0.04 g of AIBM was dissolved in 20 mL of MMA in a conical flask and the clear mixed solution was allowed to prepolymerize to generate a dense prepolymer solution in an 85 °C water bath for ~15 min under nitrogen flow. The CNT powder and the viscous prepolymerized MMA solution were hand-mixed in a ratio of 2:3 (w/w). Subsequently, a piece of copper wire (10 cm long, 150 μm diameter) was inserted into a 3.0 cm-long fused silica capillary (320 μm i.d. × 450 μm o.d., Hebei Yongnian Ruipu Chromatogram Equipment, Hebei, China) and a 2 mm opening was left in the capillary for the subsequent filling of the mixture of the prepolymerized MMA and CNT powder. The mixture was then packed into the capillary by pressing the opening end of the capillary (to a depth of ~3 mm) into a sample of the composite. The CNT-containing mixture had to touch the end of the copper wire inside the capillary to ensure electric contact, and it was then allowed to polymerize completely in a 45 °C oven for 10 h. Finally, hot-melt adhesive was applied to the open end of the capillary to glue the copper wire in place. The CNT-filled end of the electrode was successively polished with emery paper to form a disc electrode. The graphite/PMMA (graphite/PMMA = 2:3 (w/w)) composite electrode, used for comparison, was prepared by the same procedure. The surface morphologies of the PMMA sheet, CNTs, graphite/PMMA, and CNT/PMMA were observed by using a scanning electron microscope (SEM, PHILIPS XL 30). Thermal gravimetric analyses (TGA) were conducted by using a Perkin–Elmer Pyris 1 DTA-TGA instrument under nitrogen at a heating rate of 10 °C min^{-1}. XRD measurements were carried out by using a Rigaku D/max-rB diffractometer (Rigaku, Tokyo, Japan) with Cu$K_{\alpha 1}$ radiation (40 kV, 60 mA).

Apparatus: Details of the integrated microchip CE-AD system have been described previously.[31] Briefly, a homemade ±4000 V high-voltage dc power supply provided a voltage for the electrophoretic separation and the electrokinetic sample introduction. The simple-cross single-separation-channel glass microchip was obtained from Micralyne (model MC-BF4–001, Edmonton, Canada). The original detection cell was cut off, leaving the channel outlet at the end of the chip, thereby facilitating the end-column AD. The 88 mm × 16 mm chip shown in Supporting Informa-

tion Figure S2 consisted of a four-way injection cross with a separation channel of length 74 mm and injection channels of length 5 mm. The channels had a maximum depth of 20 μm and a width of 50 μm at the top. Short pipette tips were inserted into the holes of the various reservoirs. A three-dimensionally adjustable Plexiglass device for microchip CE-AD[31] was fabricated for housing the separation chip and the detector, allowing their convenient replacement, and facilitating the precise alignment between the outlet of the separation channel and the capillary-based microdisc electrode for end-column AD. Platinum wires, inserted into the individual reservoirs on the holder, served as contacts to the high-voltage power supply. A YS73–4A-3KVA alternate constant-voltage power supply (Shanghai Keyi Instrumental Factory, Shanghai, China) was employed to suppress the voltage fluctuation of the power line. To improve the reproducibility of the peak current and migration time, the whole CE system was assembled in a room that was air-conditioned at 25 °C to minimize temperature fluctuations.

Electrochemical measurements: Before use, the composite microdisc electrode was successively polished with emery paper and alumina powder, sonicated in doubly distilled water, and finally the surface of the detection electrode was positioned carefully opposite the channel outlet of the separation channel through the guiding metal tube. The gap distance between the disc electrode and the channel outlet was adjusted to approximately 50 μm by comparison with the channel width (50 μm) while being viewed under a microscope. Cyclic voltammetry (CV) and amperometric detection for microchip CE (CE-AD) were performed by using a CHI 830B electrochemical analyzer (Shanghai Chen-Hua Instruments, Shanghai, China) in combination with a three-electrode electrochemical cell consisting of a laboratory-made disc detection electrode, an auxiliary electrode, and an Ag/AgCl wire reference electrode. The electropherograms were recorded with a time resolution of 0.1 s (without any software filtration) by using the "amperometric *i–t* curve" mode while applying the detection potential. Sample injections were performed after stabilization of the baseline. All experiments were performed at room temperature.

Sample preparation: The river water was sampled from Huangpu River at Shanghai (China) and was successively filtered by using filter paper and a polypropylene filter (0.22 μm, Shanghai Bandao Industry, Shanghai, China). To minimize the differences between the water sample and the running buffer (40 mM borate buffer (pH 9.8)), an appropriate amount of borax was dissolved in the water sample to a final concentration of 10 mM and the pH value was adjusted to 9.8 with 1 M NaOH aqueous solution. The sample solution obtained was injected for the microchip-CE analysis before and directly after it was spiked with an appropriate amount of the eight phenols mentioned above.

Procedures: The CV measurements were carried out within the desired potential range at a scan rate of 100 $mV\,s^{-1}$ and no solution agitation was necessary during the run. The channels of the glass chip were treated before use by rinsing with 0.1 M NaOH and deionized water for 10 min each. The running buffers for the separation of phenols and purines were 40 mM borate buffer (pH 9.8) and a mixed solution of 10 mM borate/20 mM phosphate buffer (pH 8.0), respectively. The running-buffer reservoir and unused reservoir were filled with electrophoresis running-buffer solution, and the sample reservoir was filled with a sample solution. The detection cell was filled with the running-buffer solution. A high voltage was applied to the sample reservoir for 20 s to facilitate the filling of the injection channel, with the detection cell grounded and all the other reservoirs floating. The sample solution was loaded into the separation channel by applying an injection voltage to the sample reservoir for 3 s, with the detection cell grounded and other reservoirs floating. The separation was performed by applying a separation voltage to the running-buffer reservoir, with the detection cell grounded and other reservoirs floating.

Safety Considerations: The high-voltage power supply and associated electrical connections should be handled with extreme care to avoid electrical shock. Methyl methacrylate, 2-2′-azo-bisisobutyronitrile, and phenols are highly toxic and should be handled with extra care and in a fume hood. Skin and eye contact and accidental inhalation or ingestion should be avoided.

Acknowledgements

This work was financially supported by the Natural Science Foundation of China (NSFC 20405002 and 20675017), the Shanghai Science Committee (051107089 and 2004ZR140150212), the State Education Ministry of China, and the 863 Program of China (2004AA639740).

[1] S. Iijima, *Nature* **1991**, *354*, 56–58.
[2] R. H. Baughman, A. Zakhidov, W. A. de Heer, *Science* **2002**, *297*, 787–792.
[3] P. M. Ajayan, *Chem. Rev.* **1999**, *99*, 1787–1799.
[4] J. Wang, *Electroanalysis* **2005**, *17*, 7–14.
[5] R. S. Chen, W. H. Huang, H. Tong, Z. L. Wang, J. K. Cheng, *Anal. Chem.* **2003**, *75*, 6341–6345.
[6] C. E. Banks, T. J. Davies, G. G. Wildgoose, R. G. Compton, *Chem. Commun.* **2005**, 829–841.
[7] Z. H. Wang, J. Liu, Q. L. Liang, Y. M. Wang, G. Luo, *Analyst* **2002**, *127*, 653–658.
[8] G. Zhao, S. Q. Zang, K. Z. Liu, S. Lin, J. Liang, X. Y. Guo, Z. J. Zhang, *Anal. Lett.* **2002**, *35*, 2233–2244.
[9] J. Wang, M. Musameh, *Analyst* **2003**, *128*, 1382–1385.
[10] M. Musameh, J. Wang, A. Merkoci, Y. H. Lin, *Electrochem. Commun.* **2002**, *4*, 743–746.
[11] J. Wang, G. Chen, M. P. Chatrathi, M. Musameh, *Anal. Chem.* **2004**, *76*, 298–302.
[12] Y. D. Zhao, W. D. Zhang, H. Chen, Q. M. Luo, *Talanta* **2002**, *58*, 529–534.
[13] J. Wang, M. Musameh, *Anal. Chem.* **2003**, *75*, 2075–2079.
[14] J. Wang, M. Musameh, *Analyst* **2004**, *129*, 1–2.
[15] G. Chen, L. Y. Zhang, W. Wang, *Talanta* **2004**, *64*, 1018–1023.
[16] J. Wang, G. Chen, M. Wang, M. P. Chatrathi, *Analyst* **2004**, *129*, 512–515.
[17] H. Luo, Z. Shi, N. Li, Z. Gu, Q. Zhuang, *Anal. Chem.* **2001**, *73*, 915–920.
[18] F. H. Wu, G. C. Zhao, X. W. Wei, *Electrochem. Commun.* **2002**, *4*, 690–694.
[19] J. Wang, M. Musameh, Y. Lin, *J. Am. Chem. Soc.* **2003**, *125*, 2408–2409.
[20] M. Zhang, A. Smith, W. Gorski, *Anal. Chem.* **2004**, *76*, 5045–5050.
[21] X. L. Luo, J. J. Xu, J. L. Wang, H. Y. Chen, *Chem. Commun.* **2005**, 2169–2171.
[22] M. L. Guo, J. H. Chen, J. Li, B. Tao, S. Z. Yao, *Anal. Chim. Acta* **2005**, *532*, 71–77.
[23] M. Gao, S. Huang, L. Dai, G. Wallace, R. Gao, Z. Wang, *Angew. Chem.* **2000**, *112*, 3810–3813; *Angew. Chem. Int. Ed.* **2000**, *39*, 3664–3667.
[24] D. R. Reyes, D. Iossifidis, P. A. Auroux, A. Manz, *Anal. Chem.* **2002**, *74*, 2623–2636.
[25] P. A. Auroux, D. Iossifidis, D. R. Reyes, A. Manz, *Anal. Chem.* **2002**, *74*, 2637–2652.
[26] J. Wang, G. Chen, M. P. Chatrathi, M. Musameh, *Anal. Chem.* **2004**, *76*, 298–302.
[27] G. Chen, J. H. Li, S. Qu, D. Chen, P. Y. Yang, *J. Chromatogr.* A **2005**, *1094*, 138–147.
[28] G. Chen, Y. H. Lin, J. Wang, *Talanta* **2006**, *68*, 497–503.
[29] W. R. Vandaveer, S. A. Pasas, R. S. Martin, S. M. Lunte, *Electrophoresis* **2002**, *23*, 3667–3677.
[30] J. Wang, *Talanta* **2002**, *56*, 223–231.
[31] G. Chen, H. M. Bao, P. Y. Yang, *Electrophoresis* **2005**, *26*, 4632–4640.
[32] J. Wang, M. P. Chatrathi, B. M. Tian, *Anal. Chim. Acta* **2000**, *416*, 9–14.
[33] R. S. Martin, K. L. Ratzlaff, B. H. Huynh, S. M. Lunte, *Anal. Chem.* **2002**, *74*, 1136–1143.
[34] W. R. Vandaveer, S. A. Pasas-Farmer, D. J. Fischer, C. N. Frankenfeld, S. M. Lunte, *Electrophoresis* **2004**, *25*, 3528–3549.
[35] L. Nyholm, *Analyst* **2005**, *130*, 599–605.

[36] G. X. Xu, J. Wang, Y. Chen, L. Y. Zhang, D. R. Wang, G. Chen, *Lab Chip* **2006**, *6*, 145–148.
[37] B. Philip, J. K. Abraham, A. Chandrasekhar, V. K. Varadan, *Smart Mater. Struct.* **2003**, *12*, 935–939.
[38] W. K. Park, J. H. Kim, S. S. Lee, J. Kim, G. W. Lee, M. Park, *Macromol. Res.* **2005**, *13*, 206–211.
[39] S. J. Park, M. S. Cho, S. T. Lim, H. J. Cho, M. S. Jhon, *Macromol. Rapid Commun.* **2003**, *24*, 1070–1073.
[40] M. Cochet, W. K. Maser, A. M. Benito, M. A. Callejas, M. T. Martinez, J. M. Benoit, J. Schreiber, O. Chauvet, *Chem. Commun.* **2001**, 1450–1451.
[41] J. H. Sung, H. S. Kim, H. J. Jin, H. J. Choi, I. J. Chin, *Macromolecules* **2004**, *37*, 9899–9902.
[42] J. Wang, M. P. Chatrathi, B. M. Tian, R. Polsky, *Electroanalysis* **2000**, *12*, 691–694.
[43] M. Pumera, X. Llopis, A. Merkoci, S. Alegret, *Microchim. Acta* **2006**, *152*, 261–265.
[44] M. Chicharro, A. E. Sanchez, Bermejo, A. Zapardiel, M. D. Rubianes, G. A. Rivas, *Anal. Chim. Acta* **2005**, *543*, 84–91.
[45] R. R. Moore, C. E. Banks, R. G. Compton, *Anal. Chem.* **2004**, *76*, 2677–2682.
[46] C. E. Banks, R. G. Compton, *Analyst* **2005**, *130*, 1232–1239.

Received: April 4, 2006
Published online: October 18, 2006

